

1 *Supporting information*

2

3 **Design of a 3D Nanowire-CuO/LDH@FeNi- γ Al₂O₃ Catalyst and Its Synergistic Mechanism**
4 **for Accelerated Dye Degradation in Wastewater**

5

6 Guene L. Razack^{a,b,c,d}, Jie Ding^{a,b,*}, Xian Zhao^{a,b}, Ya-Ni Zang^{a,b}, Chen-Hao Cui^{a,b}, Wen-Shuo
7 Wang^a, Ji-Wei Pang^e, Lu-Yan Zhang^f, Worou Chabi Noel^{c,d}, Assogba Dou Rached^{c,d}, Nan-Qi
8 Ren^{a,b}, Shan-Shan Yang^{a,b,*}

9

10 *^aNational Engineering Research Center for Safe Disposal and Resources Recovery of Sludge,*
11 *Harbin Institute of Technology, Harbin 150090, China*

12 *^bState Key Laboratory of Urban-rural Water Resource and Environment, School of Environment,*
13 *Harbin Institute of Technology, Harbin 150090, China*

14 *^cLaboratory of Materials and Structures (LAMS). Graduate School of Civil Engineering*
15 *Véréchaguine, 02 BP 244 Cotonou, Benin*

16 *^dLaboratory of Water Science and Technology, National Water Institute (INE), University of*
17 *Abomey-Calavi, 01 BP 526 Cotonou, Benin.*

18 *^eHarbin Corner Science & Technology Inc., Harbin 150023, China*

19 *^fSchool of Environmental Science and Engineering, Yancheng Institute of Technology, Yancheng*
20 *224051, China*

21 **Corresponding authors: Shan-Shan Yang, shanshanyang@hit.edu.cn;*
22 *Jie Ding, dingjie123@hit.edu.cn.*

23

24 **Test S1.** Chemicals and Materials

25 The copper foam was sourced from [Kunshan Jiayixing Electronic Technology Co., LTD.](#) $\gamma\text{Al}_2\text{O}_3$
26 was obtained from [Shanghai Yaoyi Alloy Material Co., LTD.](#) Sodium Hydroxide (NaOH, 100%),
27 and ammonium Persulfate $(\text{NH}_4)_2\text{S}_2\text{O}_8$, 99% were provided by [Tianjin Tianli reagent Co., LTD.](#)
28 Nickel nitrate hexahydrate $(\text{Ni}(\text{NO}_3)_2 \cdot 6\text{H}_2\text{O}$, 98%) was supplied by [Chemical Reagent Co, LTD.](#)
29 Ferrous Sulphate $(\text{FeSO}_4 \cdot 7\text{H}_2\text{O}$, $\geq 99\%$) was acquired from [Tianjin BASF Chemical Co., LTD.](#)
30 Additionally, hydrochloric acid (HCl, 33%), acetone, and anhydrous ethanol (EtOH, $\geq 99.8\%$),
31 were obtained from [Macklin Reagent Co., LTD.](#) Rhodamine B (RhB) 95% was supplied by
32 [MIKA-Aiochemika Reagent Co., LTD](#), with acid yellow (AY) 36 and methyl blue (MB) provided
33 by [Sigma-Aldrich Co., LTD.](#) N, N-dimethylformamide $(\text{HCON}(\text{CH}_3)_2$, 99.5%) from [Tianyang](#)
34 [Tianli Chemical Reagent Co., Ltd](#), Sodium carbonate (Na_2CO_3) , sodium chloride $(\text{NaCl}, \geq 99.5\%)$,
35 [Tianjin Tianli Chemical Reagent Co., Ltd](#), sodium bicarbonate (NaHCO_3) , Sodium nitrate
36 (NaNO_3) , [Tianjin Yongda Chemical Reagent Co., Ltd](#), chloroform (CF, $\geq 99.0\%$), L-Histidine (L-
37 H), and tert-butanol (TBA) were purchased from [Sinopharm Chemical Reagent Co., Ltd.](#)
38 ([Shanghai, China](#)). Deionized water, used in all experiments, was obtained from a Milli-Q
39 academic system. All the chemicals were analytical grade without further purification.

40 **Table S1** Several chemical names and abbreviations

Chemical	Nam	Abbreviation
$\gamma\text{Al}_2\text{O}_3$	Alamina	$\gamma\text{Al}_2\text{O}_3$
Fe	iron	F
Ni	Nickel	N
Cu	Copper	C
O	Oxygen	O
LDH	Double-layer hydrogen	L
$\gamma\text{Al}_2\text{O}_3\text{xFeNiCu-LDH@CuO}$	Material	$\gamma\text{Al}_2\text{O}_3\text{xFNCL@CuO}$

41

42

43 **Test S2.** Methods and calculations of the performance removal rate analysis

44 The removal rate of RhB, MB, and AY, noted as X_{RhB}, X_{MB}, and X_{AY}, was defined according

45 to Eq. (S1-S3) respectively.

$$46 x_{RhB} = \frac{[RhB]_0 - [RhB]_t}{[RhB]_0} * 100\% \quad (S1)$$

$$47 x_{MB} = \frac{[MB]_0 - [MB]_t}{[MB]_0} * 100\% \quad (S2)$$

$$48 x_{AY} = \frac{[AY]_0 - [AY]_t}{[AY]_0} * 100\% \quad (S3)$$

49 In the context of dye wastewater treatment, X_{RhB}, X_{MB}, and X_{AY} denote the removal efficiency of
50 RhB, MB, and AY, respectively. The variables [RhB]₀, [MB]₀, and [AY]₀ represent the initial
51 concentrations of RhB, MB, and AY in the coking wastewater, whereas [RhB]_t, [MB]_t, and [AY]_t
52 refer to the residual concentrations of RhB, MB, and AY, respectively, following the 3D particle
53 electrode treatment. Subsequently, the residual concentration of Rhodamine B, methyl blue, and
54 yellow acid in the solution was determined using a TU-1901 UV-vis spectrophotometer at a
55 wavelength of 550 nm, 650 nm, and 435 nm through colorimetric analysis. The values of UV₅₅₀,
56 UV₆₅₀, and UV₄₃₅ were determined using the following equations: S(4-6):

$$57 RhB:UV_{570} = \frac{A}{b} * C \quad (S4)$$

$$58 MB:UV_{600} = \frac{A}{b} * C \quad (S5)$$

$$59 YA:UV_{435} = \frac{A}{b} * C \quad (S6)$$

60 In this equation, C_t (mg/L) denotes the RhB, MB, or AY concentration of the dye wastewater at a
61 given time, t . C_0 (mg L⁻¹) represents the initial concentration of RhB, MB, or AY in the dye
62 wastewater. The parameter k is the pseudo-first-order rate constant, expressed in minutes per min

63 Eq. (S7):

64
$$\ln C_t = -kt + \ln C_0 \quad (S7)$$

65 where C_t (mg/L) is the RhB, MB, or AY concentration of the dye wastewater at time t ; C_0 (mg L⁻¹) is the RhB, MB, or AY concentration of the dye wastewater at the initial time; and k is the
66 pseudo-first-order rate constant (min⁻¹).
67

68

69 **Test S3.** CV and EIS electrocatalysts test sample preparation

70 The electrode materials are evaluated for their electrochemical properties using the CHI760E
71 electrochemical working station. In the course of each electrochemical evaluation, encompassing
72 both cyclic voltammetry (CV) and electrochemical impedance spectroscopy (EIS), the electrolyte,
73 counter electrode, and reference electrode were consistently established as 5 M KOH aqueous
74 solution, Pt wire, and Hg/HgO electrode, respectively. The substance contained within the
75 electrode system has a loading mass of approximately 7 mg. The utilized electrolyte was 5 M
76 KOH.

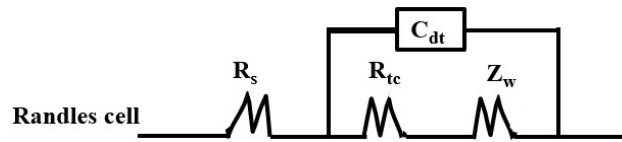
77 The three-electrode system is utilized in the test. The reference electrode employed is Hg/HgO,
78 and the counter electrode is platinum.

79 The EIS test was conducted within the frequency range of 100 kHz to 0.1 Hz, with an amplitude
80 ranging from 10 to 40 mV.

81

82 **Test S4.** EIS electroanalytical methods

83 According to [Uygun et al.¹](#), the electron-injection system (EIS) circuit and the redox reaction
84 occur at the surface of the working electrodes in a conventional electrochemical cell, otherwise
85 known as a three-electrode system. R_{ct} is an abbreviation for "charge transfer resistance," R_s is
86 an abbreviation for "electrolyte resistance," and C_{dt} is an abbreviation for "capacitance double
87 layer."



89 **Fig. S1.** The scheme is described as straightforward of the EIS circuit and the redox reaction that
90 occurs at the surface of working electrodes in a traditional electrochemical cell.

91

92 Equation S8 quantifies the correlation between the applied frequency (f) and the radial frequency
93 (ω).

94 $w = 2 \cdot \pi \cdot f$ (S8)

95 In a linear system, the signal undergoes a phase shift (Φ) and exhibits a variation in amplitude
96 relative to I_0 (Equation S9).

97 $I_t = I_0 \sin(wt + \Phi)$ (S9)

98 Therefore, as indicated by Equation S10, the impedance of the entire system can be calculated.

99 Substituting z for E and I , we obtain the following equation:

100
$$z = \frac{E}{I} = z_0 \exp(i\Phi) = z_0(\cos \Phi + i \sin \Phi)$$
 (S10)

101 The variables Z , E , I , ω , and Φ represent impedance, potential, current, frequency, and phase
102 shifts, respectively, between E and I .

103

104

105 **Test S5.** Quenching information

106 The quenching experiment is analogous to the oxidation experiment of RhB, with the salient
107 difference being the simultaneous addition of quenching, an anion molecule, and an organic
108 compound. This method has been employed by Jinxiang et al.². Quenching experiments were
109 performed with the addition of NO_3^- , Cl^- , $\text{HCO}_3^-/\text{CO}_3^{2-}$, and TBA, which were employed as
110 scavengers for nitrate radicals (NO_3^-), chlorine radical (Cl^-), carbonate radical (CO_3^{2-}), and organic
111 TBA, respectively. The quenching experiment was conducted at room temperature in 250-mL
112 clear glass beakers, with the stirring rate maintained at a constant level. Subsequently, 150 mg/L
113 of $\gamma\text{Al}_2\text{O}_3\text{xFNCL}_{20}\text{@CuO-400}$ catalysts were added to a solution containing 20 mg/ L RhB, and
114 the mixture was stirred. The pH value of the solutions was then adjusted to 8.0. The initiation of
115 the reaction was facilitated by the incorporation of 0.25, 0.50, 1, and 2 mM quenchers, along with
116 12 V, within a 3D system. Samples were collected and quenched after reacting for a specific time.
117 Subsequently, the solution was filtered with a 0.22-micrometer membrane to remove the catalysts
118 before analysis.

119

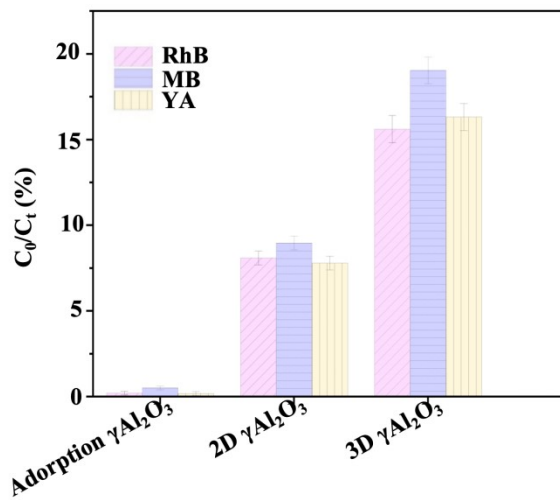
120

121

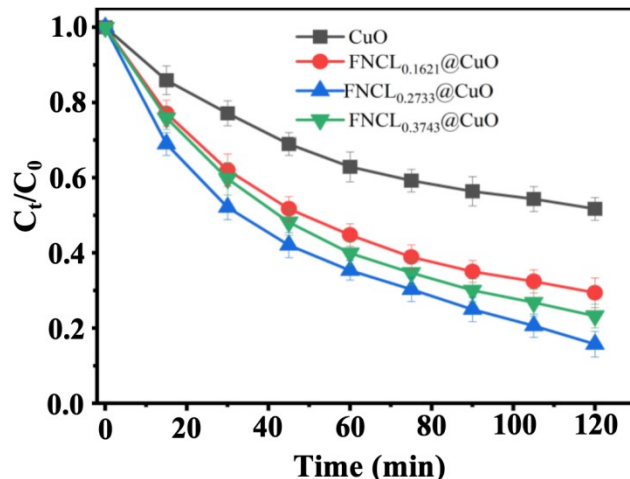
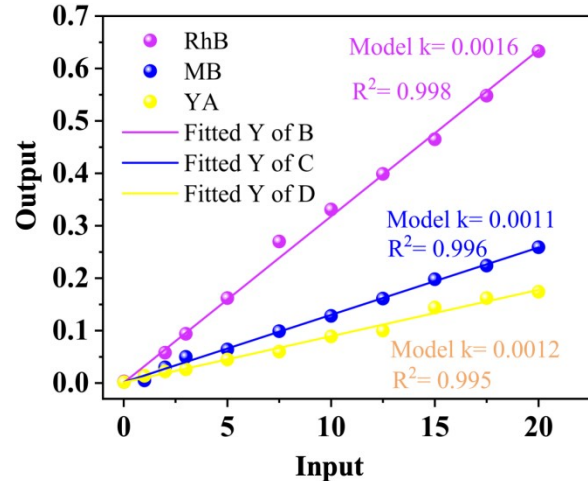
122

123

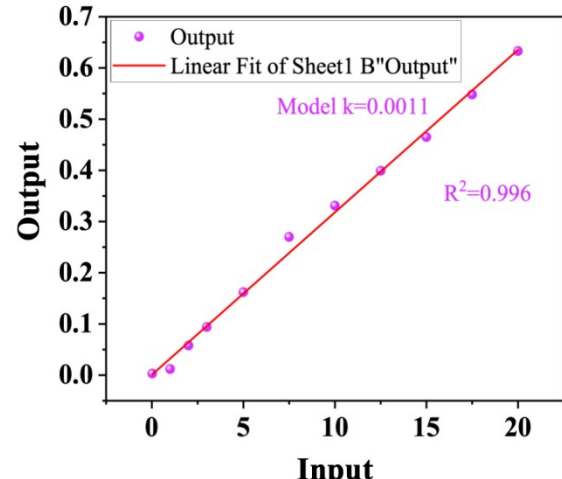
124

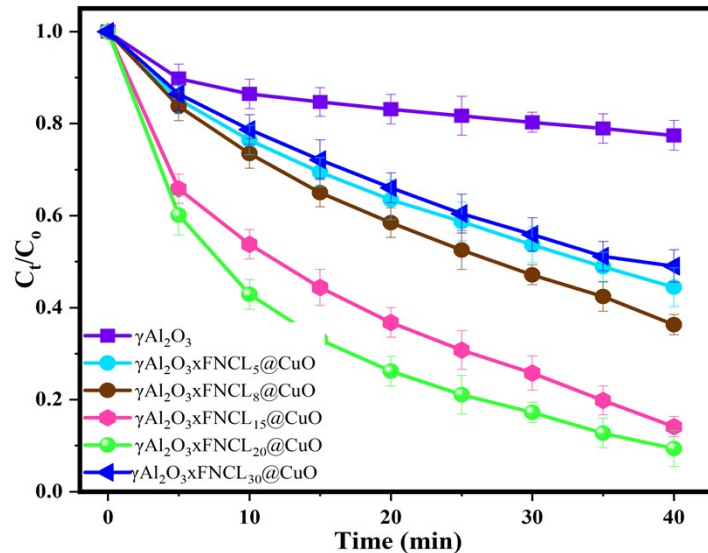
126 **2. Removal efficiency of the RhB, MB, and AY using the different catalysts**

128 **Fig. S2.** Performance removal of RhB, MB, and AY using $\gamma\text{Al}_2\text{O}_3$ catalytic, initial condition: 20
129 mg L⁻¹ of RhB, MB, and YA, 12V, at lab temperature.

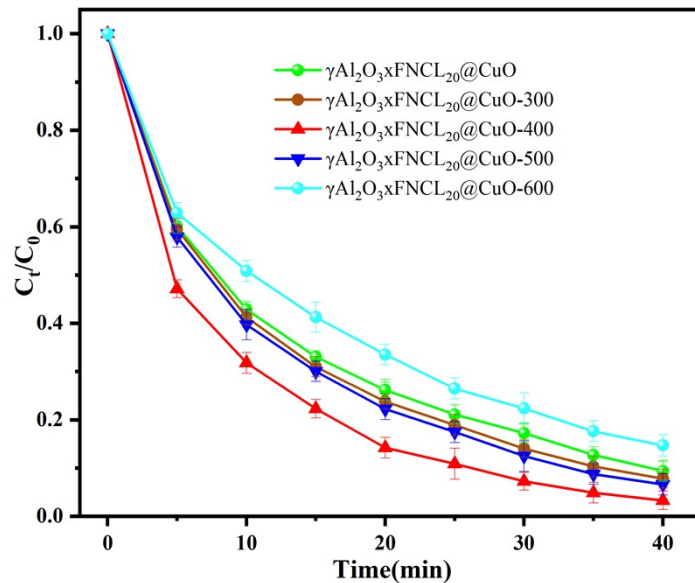


131 **Fig. S3.** performance of the different catalytic FeNiCu-LDH@CuO-0.1621, FNCL@CuO-
132 0.2733, and FNCL@CuO-0.3742 using a 3D electrode to remove RhB, MB, and AY, initial
133 condition: 20 mg L⁻¹ of RhB, 12V, at lab temperature.





136 **Fig. S4.** The removal performance of the different concentrations $\gamma\text{Al}_2\text{O}_3\text{xFNCL}@\text{CuO}$, initial
137 condition: 20 mg L^{-1} of RhB, 12 V, at lab temperature



140 **Fig. S5.** The calcination removal performance of RhB from wastewater using the 3D system,
 141 initial condition: 20 mg L⁻¹ of RhB, 12 V, at lab temperature

142 **Table S2** The performance removal of the catalysts in the 3D system.

Materials	system	Removal rate (%)		
		RhB	MB	AY
$\gamma\text{Al}_2\text{O}_3$	Adsorption	8.08	8.95	7.78
	Without $\gamma\text{Al}_2\text{O}_3$	10.53	12.82	10.62
	3D	15.6	19.03	16.3
FNCL _{0.1621} @CuO	3D	70.6	-	-
FNCL _{0.2733} @CuO	3D	84.27	-	-
FNCL _{0.3742} @CuO	3D	76.8	-	-
$\gamma\text{Al}_2\text{O}_3$ xFNCL ₅ @CuO	3D	55.55	-	-
$\gamma\text{Al}_2\text{O}_3$ xFNCL ₈ @CuO	3D	63.7	-	-
$\gamma\text{Al}_2\text{O}_3$ xFNCL ₁₅ @CuO	3D	85.85	-	-
$\gamma\text{Al}_2\text{O}_3$ xFNCL ₂₀ @CuO	3D	90.6	-	-
$\gamma\text{Al}_2\text{O}_3$ xFNCL ₃₀ @CuO	3D	50.96	-	-
$\gamma\text{Al}_2\text{O}_3$ xFNCL ₂₀ @CuO-300	3D	79.52	-	-
$\gamma\text{Al}_2\text{O}_3$ xFNCL ₂₀ @CuO-400	3D	96.69	-	-
$\gamma\text{Al}_2\text{O}_3$ xFNCL ₂₀ @CuO-500	3D	88.38	-	-
$\gamma\text{Al}_2\text{O}_3$ xFNCL ₂₀ @CuO-600	3D	85.30	-	-

143

144 3. Characterization of the new particle electrode synthesized

145 **Table S3** Physical parameters of catalysts

Catalysts	Al (At. %)	O (At. %)	Fe (At. %)	Ni (At. %)	Cu (At. %)
$\gamma\text{Al}_2\text{O}_3$	56	64	N. A ^a	N. A ^a	N. A ^a
FNCL ₂₀ @CuO	N. A	16.3	38.5	27.5	18.7
$\gamma\text{Al}_2\text{O}_3$ xFNCL@CuO-400	41.8	47.2	5.9	2.8	2.3

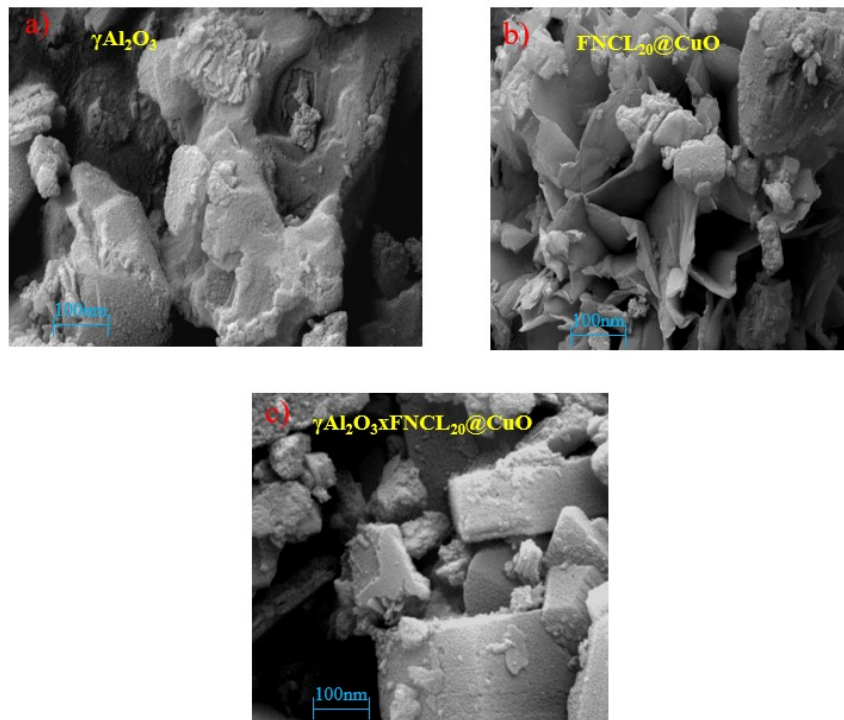
146 Note: ^a Not added

147 **Table S4** Physical parameters and lattice parameters of catalysts

Catalysts	Pore volume (cm ³ .g ⁻¹)	S _{BET} (m ² .g ⁻¹)	Average pore diameter (nm)	Lattice parameters
-----------	---	---	----------------------------	--------------------

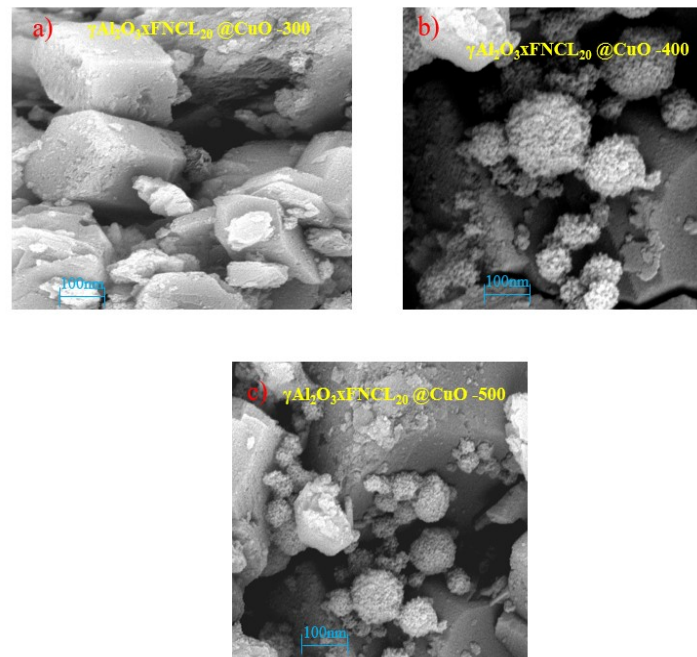
				(%)
$\gamma\text{Al}_2\text{O}_3$	0.11	15	12.4	8.5
$\gamma\text{Al}_2\text{O}_3\text{xFNCL@CuO-400}$	0.99	127	7.8	8.2

148



149
150

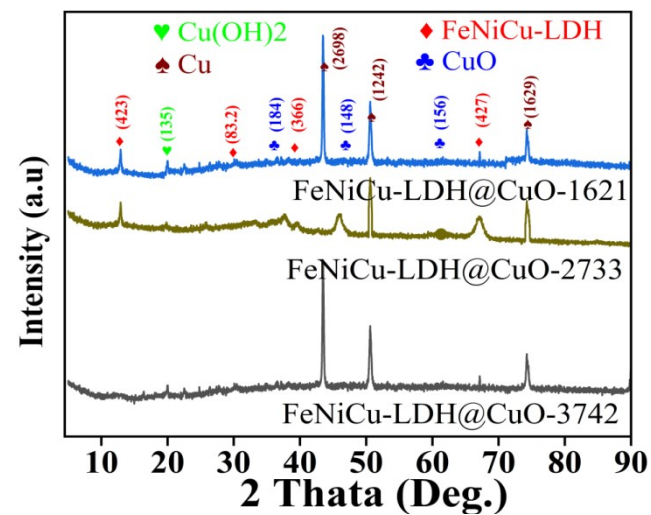
Fig. S6. Scanning electron microscope (SEM) images at 100 nm of the a) $\gamma\text{Al}_2\text{O}_3$: b)
151 FNCL@CuO, c) $\gamma\text{Al}_2\text{O}_3\text{xFNCL}_{20}\text{@CuO}$.



152

153 **Fig. S7.** Scanning electron microscope (SEM) images at 100 nm of the different calcination: a)
154 $\gamma\text{Al}_2\text{O}_3\text{xFNCL}_{20}\text{@CuO-300}$, b) $\gamma\text{Al}_2\text{O}_3\text{xFNCL}_{20}\text{@CuO-400}$, c) $\gamma\text{Al}_2\text{O}_3\text{xFNCL}_{20}\text{@CuO-500}$.

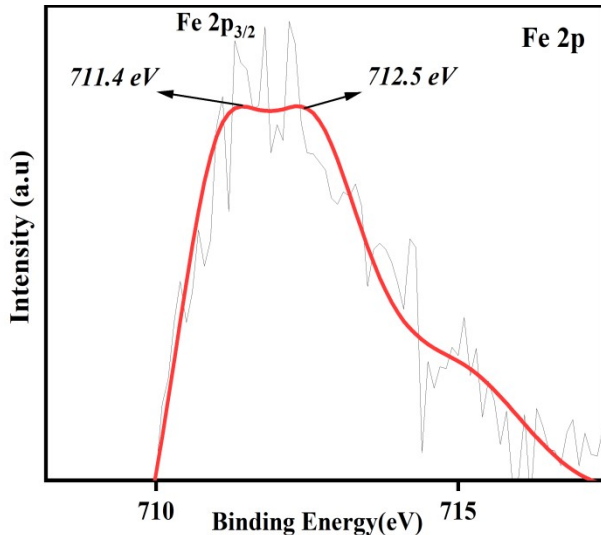
155



156

157 **Fig. S8.** XRD of the FeNiCu-LDH@CuO particle electrode

158



159

160 **Fig. S9.** Characterization XPS (Fe 2p) of the particle electrode $\gamma\text{Al}_2\text{O}_3\text{xFNCL}_{20}\text{@CuO-400}$

161

162

163 **4. Mechanism of the degradation of organic pollutants from wastewater**

164 **Table S5** A summary of the removal efficiency of the metal- Al_2O_3 electrode reported in the

165 preview literature and obtained in this study.

Catalyst	Electrode	Pollutant	Condition	Removal efficient	Reference
$\gamma\text{Al}_2\text{O}_3\text{xFNCL}@\text{CuO}$	A: Pt ^e C: Pt	RhB ^a	J: 12 V; Catalyst: 150 mg L ⁻¹ ;	98.82%, 99.99%, 98.97%.	This study
		MB ^b	Co: 20 mg L ⁻¹ ; RhB pH: 8; MB		
		YA ^c	and YA pH: 5; Time: 40 min; T: 25 °C		
$\text{CuFe}_2\text{O}_4/\text{Al}_2\text{O}_3$	A: Ti/RuO ₂ C: stain-less-steel	p-nitrophenol	24 mA cm ⁻² ; CFO/PEs dosage: 0.3 kg L ⁻¹ ; Conditions:	80.23%	3

			[PNP] = 150 mg L ⁻¹ ; pH: 4.95; T: 30 min
Bi-Sn-Sb/ γ -Al ₂ O ₃	----- ----- Bi-Sn-Sb/ γ -Al ₂ O ₃	tetracycline ciprofloxacin	I: 0.1 A; Co: 100 mg L ⁻¹ ; Particle dosage: 15 g; pH: 5.9; time 180 min
Co-Ce-Zr/ γ -Al ₂ O ₃	A: RuO ₂ - IrO ₂ /Ti C: RuO ₂ - IrO ₂ /Ti	ciprofloxacin IrO ₂ /Ti	I: 0.2 A; PEs: 15 g; Co: 100 mg L ⁻¹ ; pH: 6; T: 40 min
Ti-Sn-Sb/ γ -Al ₂ O ₃ Ti-Sn-Sb/ γ -Al ₂ O ₃	Oxytetracycline total organic carbon	I: 0.5 mA.cm ⁻² ; PEs: 20 g; Co: 100 mg L ⁻¹ ; pH: 6; T: 120 min

166 **Noted:** ^a Rhodamine B; ^b Methyl blue; ^c yellow acid; ^d Chemical organic demand; ^e Platinum

167

168 **Table S6** Degradation power of RhB

Name	Number of bonds	Estimated dipole moment	Molecular Formula	Molecular weight m/z	Proposed structure
RhB/P1	36	3.128	C ₂₈ H ₃₂ ClN ₂ O ₃	443	
P2	35	5.849	C ₂₆ H ₃₃ N ₂ O ₃	413	

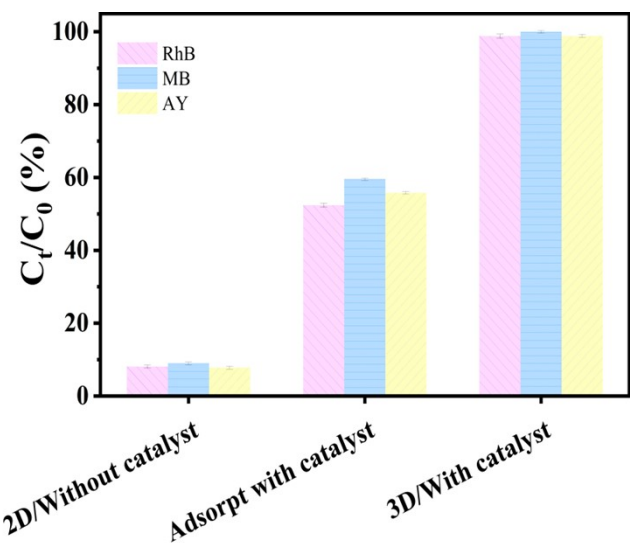
P3	31	4.403	$C_{24}H_{25}NO_3$	297	
P4	29	5.580	$C_{22}H_{21}NO_3$	327	
P5	12	4.201	$C_8H_{10}O_4$	167	
P6	9	1.954	$C_6H_{12}O_3$	132	
P7	8	2.029	$C_6H_{10}O_2$	114	
P8			$CO_2 + H_2O$	Mineralization	

169

170

171

172



173

174 **Fig. S10** 2D and 3D comparison of the performance in the removal of RhB, MB, and AY with
175 the catalyst $\gamma\text{Al}_2\text{O}_3\text{xFNL}_{20}\text{@CuO-400}$, initial condition: 150 mg L⁻¹, [catalytic]₀, 20 mg L⁻¹ of
176 [RhB]₀=[MB]₀=[YA]₀, 12 V, at lab temperature.

177

178

179

180

181

182

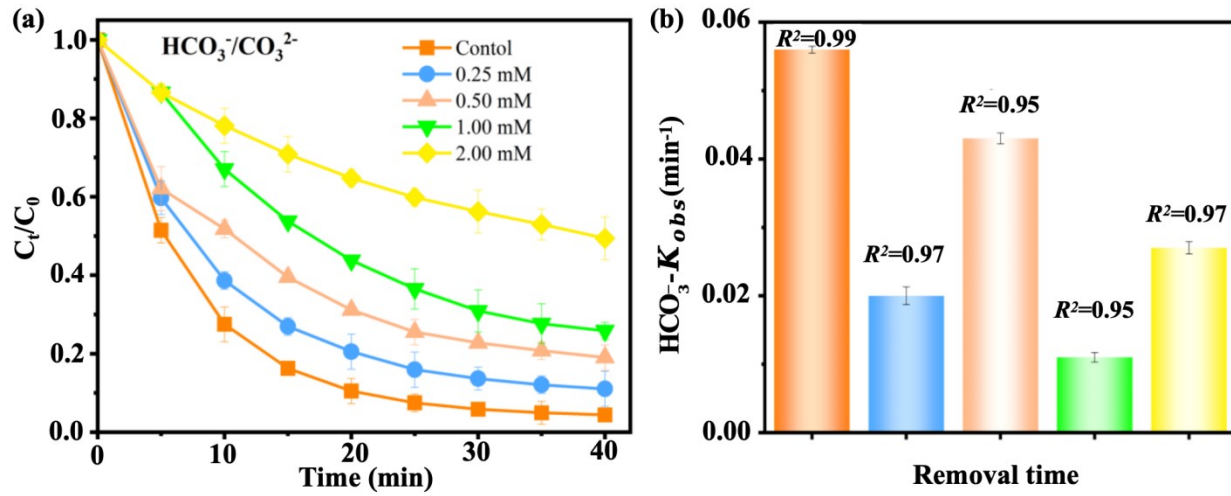
183

184

185 **Test S6** the difference in system performance

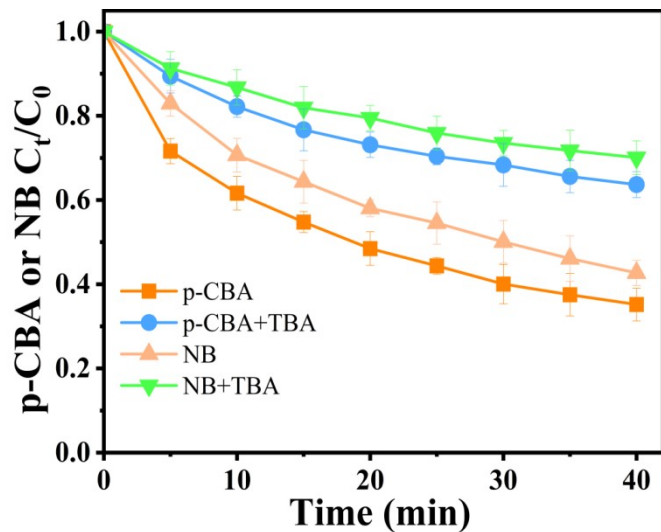
186 The variation system performance is illustrated in Figure S10, which is based on the comparative
187 results of different systems, adsorption, 2D, and 3D. According to a previous study, the production
188 of ·OH was investigated during the 2D and 3D electrolysis through the RhB degradation. As
189 demonstrated in Section 3.4, Figure 4, a greater number of hydroxyl radicals were produced after
190 40 minutes in the 3D electrolysis system compared to the 2D system. It has been demonstrated
191 that each particle electrode has the capacity to operate as a micro-electrolytic cell under
192 electrostatic induction, thereby generating an increased number of hydroxyl radicals through water
193 electrolysis in 3D electrolysis⁶. Consequently, the incorporation of suitable particle electrodes
194 within the 3D electrolysis system has been demonstrated to enhance the capacity of indirect

195 oxidation through the generation of $\cdot\text{OH}$, thereby augmenting the removal efficiency of
 196 pollutants⁷.



197

198 **Fig. S11.** (a) Effect of $\text{HCO}_3^-/\text{CO}_3^{2-}$ and the k_{obs} . (b) Duran RhB degradation using the 3D
 199 system. Conditions: $[\text{Catalyst}]_0 = 150 \text{ mg L}^{-1}$, $[\text{RhB}]_0 = 20 \text{ mg L}^{-1}$, pH = 8, and 12 V.



200

201 **Fig. S12** Oxidation of p-CBA and NB in the 3D electrode reaction without and with the addition
 202 of TBA. Conditions: $[\text{Catalyst}]_0 = 150 \text{ mg L}^{-1}$, U = 12V, $[\text{contaminants}]_0 = 20 \mu\text{M}$, $[\text{pH}]_0 = 7$, T =
 203 25 °C applied $[\text{TBA}]_0 = 100 \text{ mM}$.

205 **References**

206 1 Uygun HDE, Uygun ZO. Electrochemical Impedance Spectroscopy (EIS) Principles and
207 Biosensing Applications. Handb Nanobioelectrochemistry Appl Devices Biomol Sens.
208 2021;(2021):919–39.

209 2 Zuo J, Fu D, Yan P, Wang S, Li Y, Shen L, et al. Synergistic mechanism of surface oxygen
210 vacancies and metal sites on Al-substituted NiFe₂O₄ during peroxyomonosulfate activation
211 in the solid-water interface for 2,4-D degradation. Chem Eng J. 2024, 480, 147884.
212 //doi.org/10.1016/j.cej.2023.147884

213 3 Wu X, Song X, Chen H, Yu J. Treatment of phenolic compound wastewater using
214 CuFe₂O₄/Al₂O₃ particle electrodes in a three-dimensional electrochemical oxidation
215 system. Environ Technol (United Kingdom). 2021, 42, 393–404.
216 <https://doi.org/10.1080/09593330.2020.1760356>

217 4 Sun W, Sun Y, Shah KJ, Chiang PC, Zheng H. Electrocatalytic oxidation of tetracycline by
218 Bi-Sn-Sb/Γ-Al₂O₃ three-dimensional particle electrode. J Hazard Mater. 2019, 370, 24–32.
219 <https://doi.org/10.1016/j.jhazmat.2018.09.085>

220 5 Yixin Liu, Yongwen Ma, Jinquan Wan, Yan Wang, Jian Sun YX. Electrocatalytic oxidation
221 of ciprofloxacin by Co-Ce-Zr/γ-Al₂O₃ three-dimensional particle electrode. Environ Sci
222 Pollut Res. 2021, 28, 43815–43830. <https://doi.org/10.1007/s11356-021-13547-9>

223 6 Chao Zhang, Yonghai Jiang, Yunlin Li, Zhongxin Hu, Lei Zhou, Minghua Zhou. Three-
224 dimensional electrochemical process for wastewater treatment: A general review. Chemical

225 Engineering Journal, 2013, 228, 455-467. <http://dx.doi.org/10.1016/j.cej.2013.05.033>

226 7 Pengxiao Liu, Xu Wang, Jing Lu, Ying Li, Bin Hou, Ling Feng. Removal of antipyrine
227 through two-dimensional and three-dimensional electrolysis: comparison, modification,
228 and improvement. Environmental Science and Pollution Research, 2020, 27, 40837-40847.
229 <http://dx.doi.org/10.1007/s11356-020-09763-4>

230

231